J Mater Sci

Energy materials

Improvement of thermoelectric properties of $Ca_{0.9}Gd_{0.1}MnO_3$ by powder engineering through K_2CO_3 additions

N. M. Ferreira[1,2,*], M. C. Ferro[2], A. R. Sarabando[2], A. Ribeiro[2], A. Davarpanah[3], V. Amaral[3], M. A. Madre[4], A. V. Kovalevsky[2], M. A. Torres[4], F. M. Costa[1], and A. Sotelo[4]

[1] *i3N, Departamento de Física, Universidade de Aveiro, Campus Universitário de Santiago, 3810-193 Aveiro, Portugal*
[2] *Departamento de Engenharia de Materiais e Cerâmica, CICECO – Aveiro Institute of Materials, Universidade de Aveiro, 3810-193 Aveiro, Portugal*
[3] *Departamento de Física, CICECO – Aveiro Institute of Materials, Universidade de Aveiro, 3810-193 Aveiro, Portugal*
[4] *Dpto. de Ciencia de Materiales, ICMA (CSIC-Universidad de Zaragoza), C/María de Luna 3, 50018 Zaragoza, Spain*

Received: 24 September 2018
Accepted: 21 October 2018

ABSTRACT

Oxide materials based on calcium manganite show clear prospects as thermoelectrics, provided by their stability at high temperatures and inherent flexibility in tuning the relevant electrical and thermal transport properties. Donor-doped $CaMnO_3$ is an n-type semiconductor with a perovskite structure and relatively high thermoelectric performance. In this work, the precursor powders have been modified through potassium carbonate additions to produce $Ca_{0.9}Gd_{0.1}MnO_3$ pellets without the usual delamination problems occurring during the compaction process. In order to demonstrate the relevant effects, several samples with different amounts of potassium carbonate (0–15 wt%) have been prepared. The results showed that potassium additions significantly facilitate the compaction procedure, while also improving the thermoelectric performances. The results also highlight the importance of porosity control for improving ZT, by decreasing the thermal conductivity without reduction of the electrical performance. The highest ZT values were observed for the samples processed at 15 wt% of potassium carbonate addition, exhibiting an improvement at least 30% at 800 °C when compared to the pure samples.

Introduction

Thermoelectric (TE) materials are gaining interest due to their intrinsic advantages to increase energy transforming systems efficiency, by harvesting wasted heat into useful electric power. Among the different TE materials, oxides are among the most promising, due to their high thermal and chemical stability when working under air, and are effective at high temperatures [1]. One of the most promising

Address correspondence to E-mail: nmferreira@ua.pt

https://doi.org/10.1007/s10853-018-3058-x

Published online: 30 October 2018

compounds is $CaMnO_3$, an *n*-type semiconductor oxide with perovskite structure [2]. On the other hand, this compound possesses limited TE performances due to its low carrier concentration. Consequently, many studies have been carried out in order to improve its thermoelectric properties using dopants [1, 3]. These studies are essentially focused on the improvement of the electrical conductivity, without affecting the Seebeck coefficient or thermal conductivity [2]. The addition of dopants has already proved to increase the electrical conductivity and simultaneously reduce the thermal conductivity [4, 5].

It is known that preparation routes present a significant impact on the thermoelectric performance. Microstructural tuning is quite effective for decreasing the electrical resistivity and thermal conductivity, while increasing, or maintaining practically constant, Seebeck coefficient [6]. Consequently, in ceramic materials good and clean grain connections should be obtained to avoid adverse effects on the carrier mobility, improving the electrical conductivity without drastically modifying the thermal conductivity. Moreover, porosity control in the bulk material can help to tailor the thermal conductivity values. The formation of strong grain boundaries in relatively low density materials has already been successfully achieved in several ceramic materials [7].

On the other hand, to the best of our knowledge, the literature lacks the details about pressing procedures and associated problems. Based on our experience, obtaining green compacts from these powders and, in particular, manganites, is not a trivial task. In order to improve the compacts quality various approaches have been used, including low compaction pressures, leading, however, to low-density sintered bodies [8]; adding binders, which should be eliminated before sintering [9]; or using more complex procedures [8, 10].

Present study focuses on the modification of precursor powders of $Ca_{0.9}Gd_{0.1}MnO_3$ thermoelectric ceramics, aiming to facilitate the production of the green compacts while avoiding the previously mentioned drawbacks. Further changes should proceed during the calcining step in order to avoid any adverse effects during the sintering procedure. Taking into account the typical calcining temperature in this family (900 °C) [8, 10], K_2CO_3 is a good candidate as it melts below 900 °C [11]. Moreover, previous studies in cobaltites thermoelectric have shown that K_2CO_3 vanishes at 900 °C even during sintering of compact pellets, having no detrimental effect on the thermoelectric performances [12]. Herein, a very facile and scalable sintering method for producing highly-performing thermoelectric ceramics with controlled porosity has been developed [12] through the addition of different amounts of K_2CO_3 to the initial powders mixture. In the present work, somewhat similar approach was implemented for manganite-based ceramics. The corresponding microstructural evolution is linked to the thermoelectric performance.

Experimental

$Ca_{0.9}Gd_{0.1}MnO_3 + x$ wt% K_2CO_3 samples (x = 0, 5, 10, and 15) were prepared using $CaCO_3$ (Panreac, 99,5%), MnO (Panreac, 99%), Gd_2O_3 (Aldrich, 99,9%), and K_2CO_3 (Panreac, 99%) commercial powders. They were weighed in stoichiometric proportions, and ball milled in aqueous media for 30 min at 300 rpm. The resulting suspension was dried using a rapid infrared evaporation system described elsewhere [12]. Some part of the powders obtained after water evaporation was kept for further characterization. The other part was calcined at 900 °C for 12 h, to decompose the carbonates ($CaCO_3$ and K_2CO_3), as reported in previous works [12, 13]. After grinding in the mortar, these powders were uniaxially cold pressed at 400 MPa in form of pellets ($3 \times 3 \times 14$ mm^3) which were then sintered at 1300 °C for 24 h, with a final furnace cooling. It is worth to mention that the pellets with at least 10 wt% K_2CO_3 content have been easily obtained, while for lower additions PVA (PolyVinyl Alcohol) has to be added as a binder to facilitate the compaction. Otherwise the delamination was observed, as illustrated in Fig. 1.

Powder X-ray diffraction (XRD) analysis was performed between 10° and 70° from room temperature until 1200 °C, using a Panalytical X'pert PRO3 (CuKα1 radiation) with a temperature chamber from Anton Paar, on the dry powders after milling procedure to evaluate the relevant effects of potassium carbonate addition. The carbonate decomposition has been studied by FTIR analysis using a Bruker IFS 28 Spectrometer, on calcined powders. Moreover, particle size distribution has also been performed on these powders using a laser beam diffraction method,

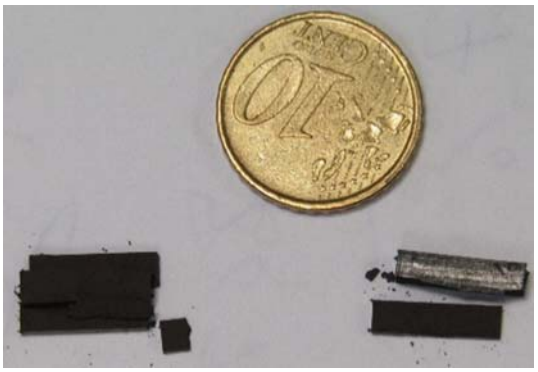

Figure 1 Photograph showing the delamination of bars after pressing the powders without additions.

with a Coulter LS230 equipment at room temperature. This technique is based on the Fraunhoffer diffraction principle, which allows evaluating the particle size as a function of a laser beam diffraction angle when it crosses a set of particles.

Phase identification of the sintered materials was performed by powder XRD at room temperature, using the similar experimental procedure as described above.

Microstructural studies were performed in a FESEM (Zeiss Merlin) on calcined powders to observe the grains evolution with the K_2CO_3 content. Moreover, longitudinal polished sections of samples were studied in a SEM (Su-70, Hitachi) equipped with an energy dispersive spectrometry (EDS) system (Bruker) in order to determine the phases content and distribution. Apparent density was measured on bulk sintered samples, using Archimedes method at room temperature.

Electrical resistivity and Seebeck coefficient were simultaneously measured on sintered samples, using the steady state mode, by the standard DC four-probe technique in a LSR-3 apparatus (Linseis GmbH) between 50 and 800 °C under He atmosphere. Thermal conductivity measurements were performed at room temperature, using a transient plane source technique (Hot Disk TPS 2500 s). This method involves an electrically conducting element, acting both as a temperature sensor and heat source, insulated with two thin layers of Kapton (70 μm).The transient plane source element is sandwiched between two similar samples, with both faces being in contact with the samples surfaces.

Finally, figure of merit (ZT) was calculated, using electrical resistivity, Seebeck coefficient, and thermal conductivity data. It should be noticed that the thermal conductivity value, measured at room temperature, was used for ZT estimation at higher temperatures, assuming the thermal conductivity constant, independently of the temperature [12]. This rough assumption leads to clear underestimation of the real ZT values, as the thermal conductivity of manganites is decreasing when the temperature is raised [14, 15], but in the present work it was used for comparison purposes.

Results and discussion

The results of SEM analysis of the powders after calcination clearly illustrate the effect of potassium carbonate additions on the $Ca_{0.9}Gd_{0.1}MnO_3$ microstructure, as shown in Fig. 2. K_2CO_3 promotes a significant coalescence of the particles up to 10 wt%, leading to large particles agglomerates with individual sizes larger than 500 nm. On the other hand, higher K_2CO_3 content increases the agglomerates sizes, as well as the size of the individual particles.

Particle size analysis, presented in Fig. 3 has shown that the samples containing 10 wt% of K_2CO_3 present the highest mean particle diameter, while samples without additions present the lowest particle diameters. These results clearly indicate the influence of potassium carbonate which promotes the grain growth during the calcination procedure.

In order to determine if carbonates are still present on the samples after calcination, FTIR analysis was performed on all samples and the results are presented in Fig. 4. Two strong bands at 1635 and 1415 cm^{-1} represent the vibration for the ionized carboxylate symmetric and asymmetric C–O stretching [16, 17].Furthermore, the content of calcium and potassium carbonates increased with K_2CO_3 load. This effect can be attributed to the fact that the calcination process was performed under static air. Consequently, the CO_2 partial pressure on the atmosphere in close contact with the powders is raised, hindering the total carbonate decomposition.

The effect of temperature on the powders evolution has been further evaluated by XRD analysis at different temperatures, and the obtained patterns are presented in Fig. 5 for the samples without (0 wt%) and with 10 wt% K_2CO_3 addition. As it can be deduced from the diffractograms presented in the figure, both samples evolve differently, illustrating

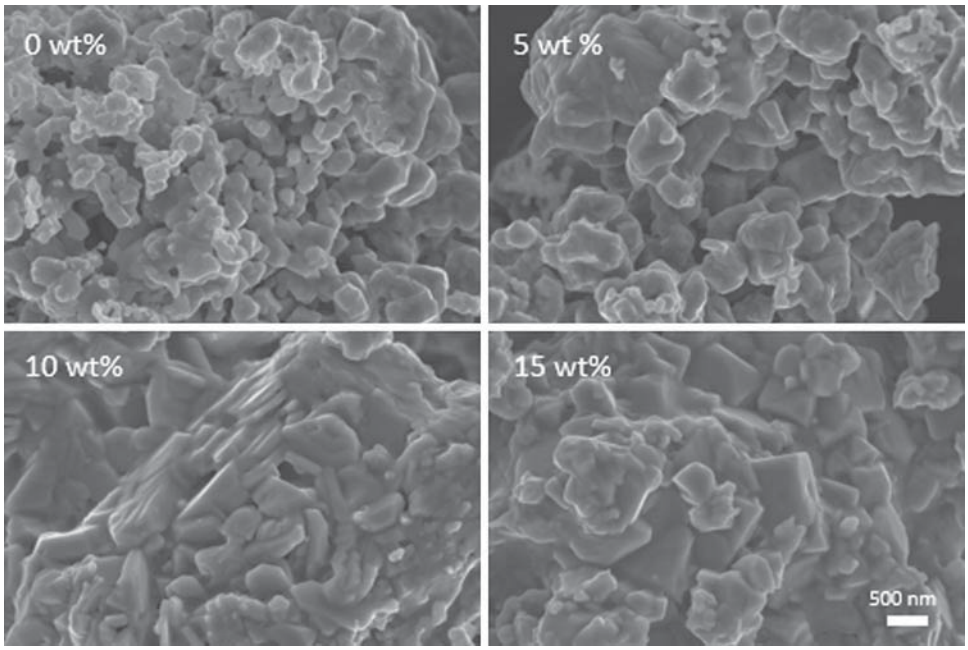

Figure 2 SEM micrographs of the powders with various K_2CO_3 addition content after calcination at 900 °C for 12 h.

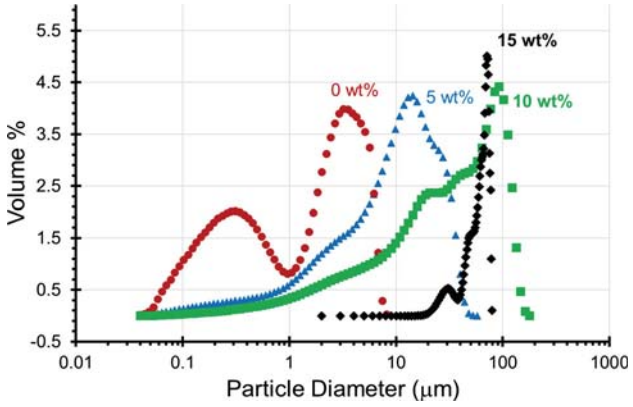

Figure 3 Dispersion of particle diameter in samples with different K_2CO_3 content.

the effect of potassium carbonate addition. K_2CO_3 addition to the initial powders promotes the formation of $CaMnO_3$ phase at low temperatures (700 °C), confirmed by the absence of this phase in the potassium-free sample. However, after reaching 1200 °C and cooling down to room temperature, several phases can be detected in all samples due to the short time heating and cooling process, which leads to incomplete reaction. It is worth to mention that these data highlight the phases evolution with temperature, but the amount of the final products after calcining procedure should be different due to the longer time and lower temperature of this process (900 °C, 12 h).

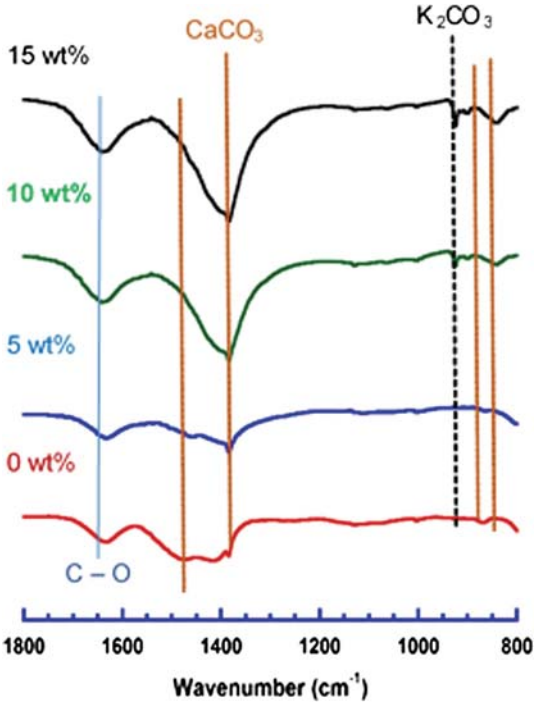

Figure 4 FTIR spectra of the powders after calcination process. The different colour and style lines identify the absorptions peaks for each compound.

After the sintering of these calcined powders at 1300 °C for 12 h, the powder XRD analysis was performed and the results are shown in Fig. 6. All samples present as the major phase $Ca_{0.9}Gd_{0.1}MnO_3$

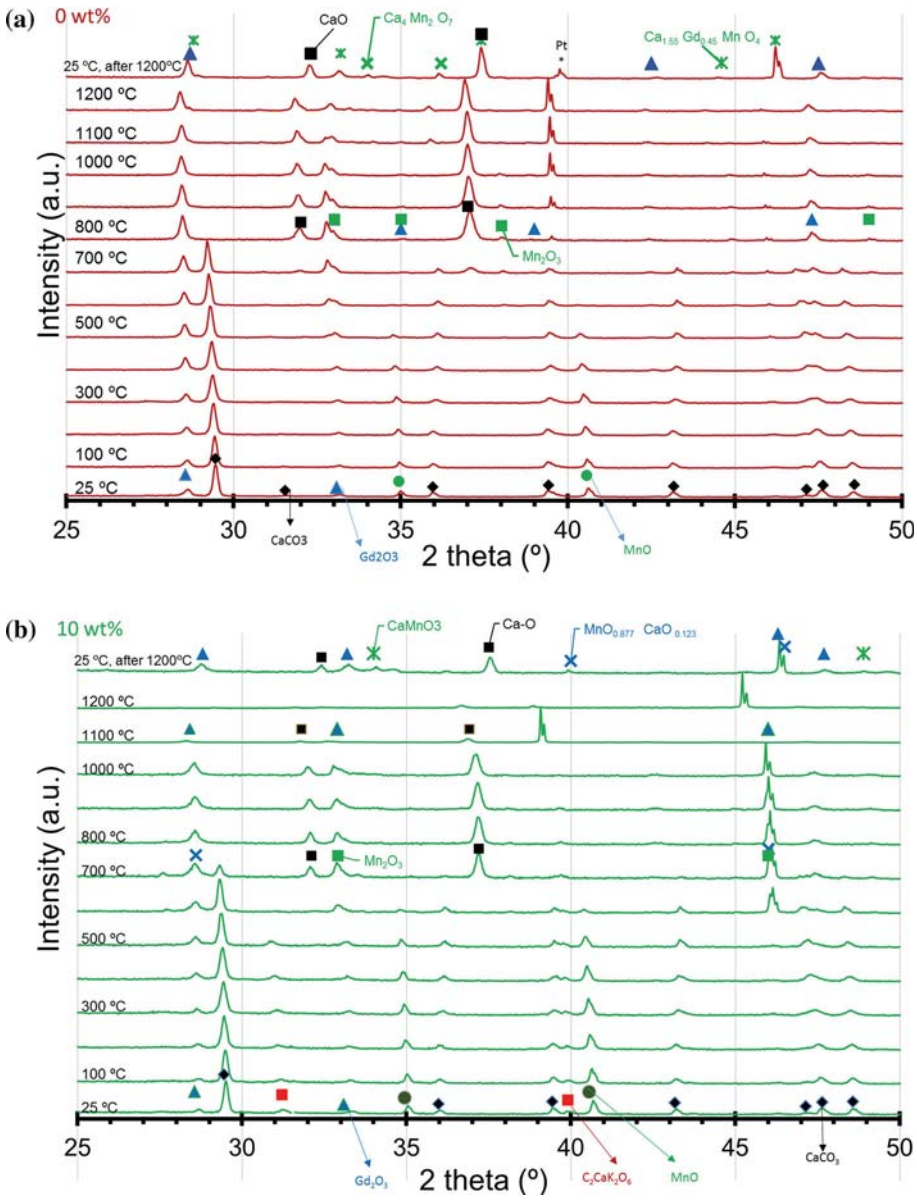

Figure 5 Powder XRD difractograms from room temperature to 1200 °C for samples with **a** 0 wt% and **b** 10 wt% K_2CO_3 addition.

(PDF card: 04-015-8452), with orthorhombic crystalline structure. Moreover, small amounts of $Ca_2Mn_2O_5$ secondary phase (card: 04-010-2534), with orthorhombic structure are also identified.

Similar phase composition was previously reported for the $CaMnO_3$ system, processed under similar thermal conditions [8]. From the results displayed in these patterns, it can be also observed that the amount of secondary phase is decreasing with potassium carbonate content. This evolution clearly evidence the influence of K_2CO_3 on the reaction kinetics to produce the thermoelectric perovskite phase, as discussed above (see Fig. 5). This effect can be promoted by the formation of a K_2CO_3-based liquid phase, which enhances cation mobility and interdiffusion during the thermal treatments [12].

The potassium carbonate additions also have an impact on the ceramics density, as displayed in Fig. 7. From these results, it is possible to observe that the increase of potassium carbonate amount in the samples first increases the density up to 5 wt%, while decreasing for higher additions. Furthermore, 5 and 10 wt% K_2CO_3—loaded samples present higher density than the sample without addition. This result can be expected if considering previous studies [18], where potassium carbonate has been mixed with copper powder to produce open pore cell structure in the bulk material after sintering. Moreover, porosity

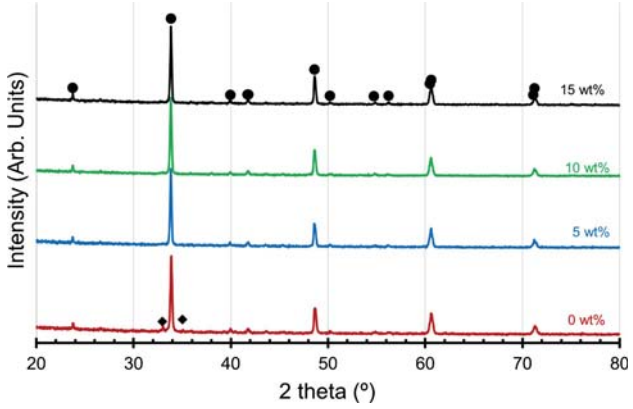

Figure 6 Powder XRD difractograms at room temperature for sintered samples with different potassium carbonate additions, • = $CaMnO_3$ phase and ◆ = $Ca_2Mn_2O_5$ secondary phase.

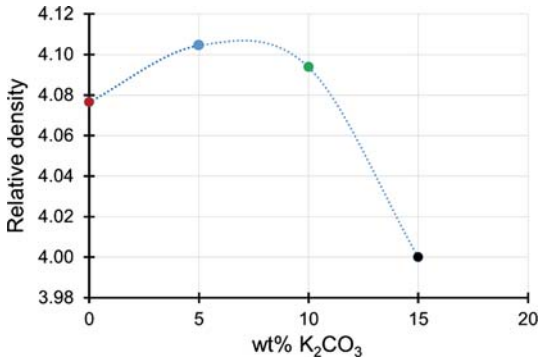

Figure 7 Relative density of samples, as a function of K_2CO_3 addition, after sintering at 1300 °C for 12 h.

volume was increased when potassium carbonate was added, corroborating the results obtained in this work.

Figure 8 shows representative micrographs of the sintered samples surfaces. These images are not conclusive regarding the effect of potassium carbonate additions on the microstructure of sintered samples. This is due to the small density variation between the different samples, as previously discussed. On the other hand, EDS analysis did not reveal the presence of potassium in the samples after sintering, indicating its total loss during this process. Taking into account that FTIR results showed that samples with 10 and 15 wt% K_2CO_3 additions still contain a fraction of potassium carbonate after calcination (see Fig. 4), it may indicate that potassium carbonate played an important role in the cations mobility during the sintering procedure.

Thermal properties of sintered samples at room temperature as a function of K_2CO_3 content are summarized in Table 1, where thermal conductivity (κ), thermal diffusivity (D) and heat capacity (C_p) values are presented. The values obtained for the thermal conductivity agree well with those reported for pure and doped $CaMnO_3$ phase [1, 19, 20]. Moreover, the thermal conductivity evolution with the K_2CO_3 content is the same observed with the samples density, clearly showing that lower porosity of samples leads to higher κ values, in agreement with previously published results [1]. This effect is because pores act as insulating medium for heat transport, limiting the thermal conductivity in the bulk samples. Thus, the highest density sample possesses the highest diffusivity, leading to the highest κ values [1, 18].

In Fig. 9, the electrical resistivity evolution of samples with temperature, as a function of K_2CO_3 content is presented. All samples present metallic behaviour in the whole measured temperature range, in accordance with the literature data [3, 6, 8, 21]. The results suggest that K_2CO_3 addition drastically decreases electrical resistivity values. This behaviour apparently illustrates the effect of a liquid phase (mainly K_2CO_3), leading to low resistivity of the grain boundaries. On the other hand, it also reflects the consequence of a liquid excess, which starts to increase the porosity in the sintered samples, with adverse effects on the electrical properties and density. The lowest values determined in this work at room temperature (∼ 4 mΩ cm) have been observed for 5 wt% K_2CO_3—loaded samples. These values are lower than those measured in sintered $CaMnO_3$ (125 mΩ cm) [22], or in spark plasma sintered (SPS) materials (10 mΩ cm) [23]. On the other hand they are within the best results observed for doped or co-doped $CaMnO_3$ (2.3–7.0 mΩ cm) [4, 24–26].

The evolution of Seebeck coefficient (S) with temperature is displayed in Fig. 10. The S values are negative at all temperatures, showing that dominant carriers are electrons in all samples. Furthermore, absolute values are increasing with the temperature, which is the typical behaviour in the manganites family [6, 21, 27, 28]. In addition, all samples display very similar values at the measured temperatures, indicating that Mn likely possesses the same oxidation states in all of them, independently of K_2CO_3 addition. The highest values at room temperature (− 80 μV/K) are clearly lower than the determined in

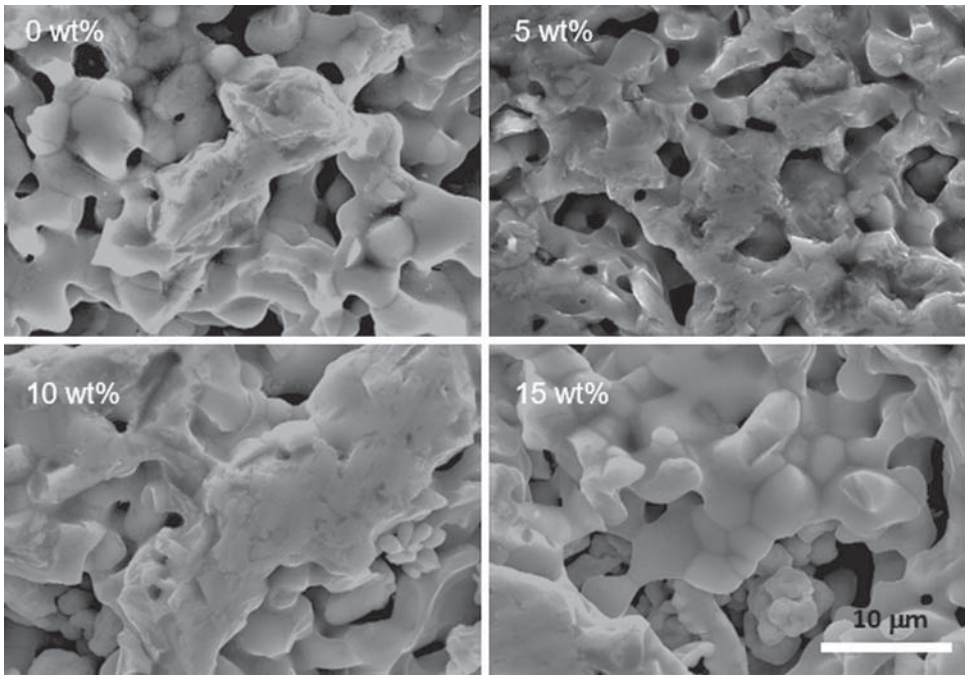

Figure 8 Representative SEM micrographs taken at the surfaces of sintered samples with different K_2CO_3 additions.

Table 1 Thermal parameters determined in the different samples at room temperature: thermal conductivity (k), thermal diffusivity (D) and heat capacity (C_p)

wt% K_2CO_3	K (W/m K)	D (mm^2/s)	C_p ($MJ/(m^3\ K)$)
0	0.64	0.49	1.33
5	1.22	0.79	1.56
10	0.91	0.57	1.62
15	0.68	0.50	1.35

pure $CaMnO_3$ (− 350 µV/K) [1], reflecting the higher carrier concentration in the doped materials. On the other hand, they are in the order of those reported in doped or co-doped materials prepared through different techniques (between − 70 and − 120 µV/K) [4, 23–26]. These results indicate that K_2CO_3 addition, besides the porosity and grains connectivity modification discussed above has negligible effect on the thermoelectric phase.

Electrical performances of the samples determined by the power factor (PF = S^2/ρ, not shown here) are within those reported in the literature [1, 28]. Moreover, the lowest values are obtained in samples without K_2CO_3 additions, while the highest were determined with 5 wt% additions, in agreement with their lower electrical resistivity.

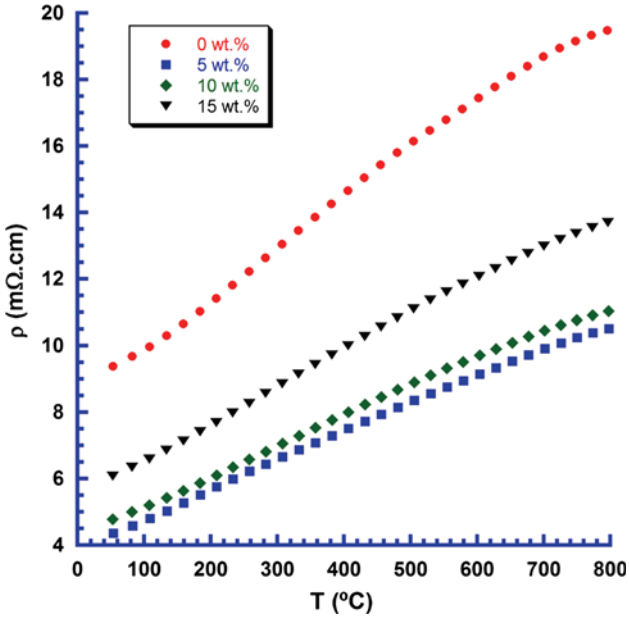

Figure 9 Electrical resistivity evolution with temperature for sintered samples with different K_2CO_3 additions.

Finally, Fig. 11 compares the thermoelectric performances of the studied samples, evaluated through their ZT. As previously mentioned in the experimental section, the ZT values at high temperatures can be significantly underestimated, since typically the thermal conductivity of manganites decreases when the temperature is raised [14, 15]. Despite of the higher electrical performances of the 5 and 10 wt%

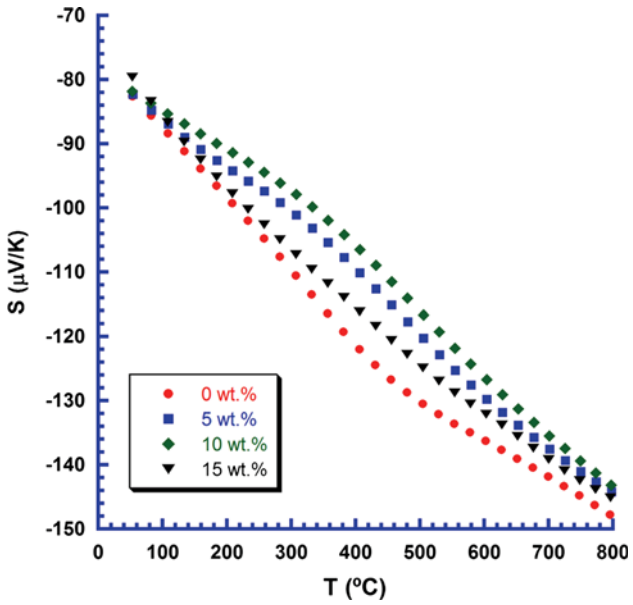

Figure 10 Evolution of Seebeck coefficient with temperature for sintered samples with different K_2CO_3 additions.

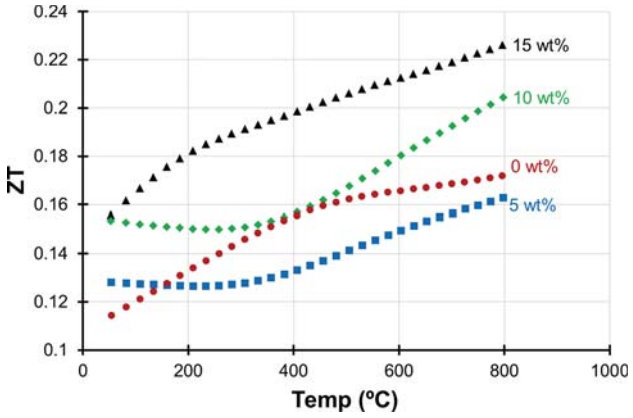

Figure 11 ZT evolution with temperature for sintered samples with different amount of K_2CO_3 addition.

K_2CO_3 samples, the highest ZT values have been determined in the 15 wt% samples, due to the lower thermal conductivity. The maximum ZT determined in this work corresponds to ~ 0.12, and 0.17 at room temperature and 800 °C, respectively. These values are within the range described in the literature for $CaMnO_3$ system [3, 27, 28].

The obtained results clearly show the benefits of K_2CO_3 addition to the initial powders, not only by facilitating the compaction of the materials, but also by increasing their thermoelectric performances thought improved grains connectivity and porosity control. This synergy appears very attractive for processing of bulk oxide thermoelectrics, where simultaneous improvement of thermoelectric properties and compaction procedure is achieved by using relatively inexpensive additions. Further efforts might be focused on the application of the proposed approach to other oxide materials with reasonable thermoelectric performance, with more emphasis on the porosity control. Such powder engineering is also expected to be attractive for ceramists focused on other applications, where powder compaction step and control of the electrical performance are crucial.

Conclusions

$Ca_{0.9}Gd_{0.1}MnO_3$ thermoelectric materials have been prepared through the classical solid state method. It has been found that K_2CO_3 addition to the precursors mixture promotes compaction without the need of organic binders, which allows to avoid the detrimental effects of organics decomposition during thermal processing. Moreover, K_2CO_3 produces the formation of a liquid phase, which enhances cation mobility and interdiffusion, reflected in higher densities (up to 10 wt%) and lower electrical resistivity, compared with the samples without additions. Microstructure and Seebeck coefficient were found to be very similar in all samples, confirming that K_2CO_3 addition has negligible effect on the thermoelectric phase. On the other hand, in spite of the large increase of thermal conductivity due to the better electrical connectivity of grains, the relatively slight decrease of density in samples with 15 wt% K_2CO_3 additions leads to thermal conductivities very similar to those measured in the pure samples. The highest thermoelectric performances have been obtained for the samples containing 15 wt% of K_2CO_3 addition, with an improvement of around 30% at 800 °C as compared to the pure samples.

Acknowledgements

N.M. Ferreira, A.V. Kovalevsky and FM Costa acknowledge the support of i3 N (UID/CTM/50025/2013) and CICECO-Aveiro Institute of Materials (UID/CTM/50011/2013), financed by FCT/MEC and FEDER under the PT2020 Partnership Agreement. The support from FCT (Portugal) grant SFRH/BPD/111460/2015, and the funding that allowed a

scientific mission to Zaragoza to perform the present work, is also acknowledged. A. Sotelo, M. A. Madre, J. C. Diez, and M. A. Torres acknowledge the Gobierno de Aragon (Grupo de Investigacion T 54-17 R), and the MINECO-FEDER (MAT2017-82183-C3-1-R) for funding.

References

[1] Kabir R, Tian R (2015) Role of Bi doping in thermoelectric properties of CaMnO3. J Alloy Compd 628:347–351

[2] Zhang FP, Lu QM, Zhang X, Zhang JX (2011) First principle investigation of electronic structure of CaMnO3 thermoelectric compound oxide. J Alloy Compd 509:542–545. https://doi.org/10.1016/j.jallcom.2010.09.102

[3] Wang H, Su W, Liu J, Wang C (2016) Recent development of n-type perovskite thermoelectrics. J Materiom 2:225–236. https://doi.org/10.1016/j.jmat.2016.06.005

[4] Flahaut D, Mihara T (2006) Thermoelectrical properties of A-site substituted Ca1-xRexMnO3 system. J Appl Phys 100:84911–84914

[5] Wang Y, Sui Y (2009) High temperature thermoelectric response of electron-doped CaMnO3. Chem Mater 21:4653–4660

[6] Sotelo A, Torres M, Madre M, Diez J (2017) Effect of synthesis process on the densification, microstructure, and electrical properties of Ca0.9Yb0.1MnO3 ceramics. Int J Appl Ceram Technol 14:1190–1196. https://doi.org/10.1111/ijac.12711

[7] Milak PC, Minatto FD, De Noni A Jr, Montedo ORK (2015) Wear performance of alumina-based ceramics—a review of the influence of microstructure on erosive wear. Cerâmica 61:88–103. https://doi.org/10.1590/0366-69132015613571871

[8] Mouyane M, Itaalit B, Bernard J, Houivet D, Noudem JG (2014) Flash combustion synthesis of electron doped-CaMnO3 thermoelectric oxides. Powder Technol 264:71–77. https://doi.org/10.1016/j.powtec.2014.05.022

[9] Taktaka R, Bakloutib S, Bouaziza J (2011) Effect of binders on microstructural and mechanical properties of sintered alumina. Mater Charact 62:912–916

[10] Melo Jorge ME, Correia dos Santos A, Nunes MR (2001) Effects of synthesis method on stoichiometry, structure and electrical conductivity of CaMnO3. Int J Inorg Mater 3:915–921

[11] http://www.chemicalbook.com/ChemicalProductProperty_EN_CB4853879.htm

[12] Sotelo A, Costa FM, Ferreira NM, Kovalevsky A, Ferro MC, Amaral VS, Amaral JS, Rasekh Sh, Torres MA, Madre MA, Diez JC (2016) Tailoring Ca3Co4O9 microstructure and performances using a transient liquid phase sintering additive. J Eur Ceram Soc 36:1025–1032. https://doi.org/10.1016/j.jeurceramsoc.2015.11.024

[13] https://pubchem.ncbi.nlm.nih.gov/compound/calcium_carbonate#section=Boiling-Point. Last visit March 2018

[14] Li C, Chen Q, Yan Y, Li Y, Zhao Y (2018) High-temperature thermoelectric properties of $Ca_{0.92}La_{0.04}RE_{0.04}MnO_3$ (RE = Sm, Dy and Yb) prepared by coprecipitation. Mater Res Express 5:25510

[15] Reimann T, Topfer J (2017) Thermoelectric properties of Gd/W double substituted calcium manganite. J Alloys Compd 699:788–795

[16] Rosić M, Kljajević LJ, Jordanov D, Stoiljković M, Kusigerski V, Spasojević V, Matović B (2015) Effects of sintering on the structural, microstructural and magnetic properties of nanoparticle manganite Ca1-xGdxMnO3 (x = 0.05; 0.1; 0.15; 0.2). Ceram Int 41:14964–14972. https://doi.org/10.1016/j.ceramint.2015.08.041

[17] Soleymani M, Moheb A, Joudaki E (2009) High surface area nano-sized La0.6Ca0.4MnO3 perovskite powder prepared by low temperature pyrolysis of a modified citrate gel. Eur J Chem 7(2009):809–817. https://doi.org/10.2478/s11532-009-0083-2

[18] Noorsyakirah A, Mazlan M, Afian OM, Aswad MA, Jabir SM, Nurazilah MZ, Afiq NHM, Bakar M, Nizam AJM, Zahid OA, Bakri MHM (2016) Application of potassium carbonate as space holder for metal injection molding process of open pore copper foam. Proc Chem 19:552–557. https://doi.org/10.1016/j.proche.2016.03.052

[19] Wang Y, Sui Y, Wang X, Su W, Liu X, Fan HJ (2010) Thermal conductivity of electron-doped CaMnO3 perovskites: local lattice distortions and optical phonon thermal excitation. Acta Mater 58:6306–6316. https://doi.org/10.1016/j.actamat.2010.07.052

[20] Baranovskiy A, Graff A, Klose J, Mayer J, Amouyal Y (2018) On the origin of vibrational properties of calcium manganate based thermoelectric compounds. Nano Energy. https://doi.org/10.1016/j.nanoen.2018.02.054

[21] Sotelo A, Depriester M, Torres MA, Sahraoui AH, Madre MA, Diez JC (2018) Effect of simultaneous K, and Yb substitution for Ca on the microstructural and thermoelectric characteristics of $CaMnO_3$ ceramics. Ceram Int. https://doi.org/10.1016/j.ceramint.2018.04.071

[22] Noudem JG, Kenfaui D, Quetel-Weben S, Sanmathi CS, Retoux R, Gomina M (2011) Spark plasma sintering of n-Type thermoelectric Ca0.95Sm0.05MnO3. J Amer Ceram Soc. 94:2608–2612

[23] Quetel-Weben S, Retoux R, Noudem JG (2013) Thermoelectric Ca0.9Yb0.1MnO3 − δ grain growth controlled by spark plasma sintering. J Eur Ceram Soc 33:1755–1762

[24] Kabir R, Wang D, Zhang T, Tian R, Donelson R, Tan TT, Li S (2014) Tunable thermoelectric properties of Ca0.9Yb0.1MnO3 through controlling the particle size via ball mill processing. Ceram Int 40:16701–16706

[25] Wang H, Wang C (2012) Synthesis of Dy doped Yb0.1Ca0.9MnO3 ceramics with a high relative density and their thermoelectric properties. Mater Res Bull 47:2252–2256

[26] Zhu Y, Wang C, Wang H, Su W, Liu J, Li J (2014) Influence of Dy/Bi dual doping on thermoelectric performance of CaMnO3 ceramics. Mater Chem Phys 144:385–389

[27] Park JW, Kwak DH, Yoon SH, Choi SC (2009) Thermoelectric properties of Bi, Nb co-substituted CaMnO3 at high temperature. J Alloy Compd 487:550–555. https://doi.org/10.1016/j.jallcom.2009.08.012

[28] Molinari M, Tompsett DA, Parker SC, Azoughb F, Freerb R (2014) Structural, electronic and thermoelectric behaviour of CaMnO3 and CaMnO(3-δ). J Mater Chem A 2:14109. https://doi.org/10.1039/c4ta01514b